The modulated crystal structure of antigorite: The *m* = 17 polysome

GIANCARLO CAPITANI* AND MARCELLO MELLINI

Dipartimento di Scienze della Terra, Via Laterina 8, 53100 Siena, Italy

ABSTRACT

The modulated crystal structure of an antigorite polysome with $m = 17$ was refined by single crystal X-ray diffraction in the *Pm* space group, using highly ordered single crystals from Val Malenco, Italy. The chemical composition is $(Mg_{2.673}Fe^{2+}_{0.098}Fe^{3+}_{0.015}Al_{0.035}Cr_{0.007}Ni_{0.003}Mn_{0.002})_{\Sigma=2.823}(Si_{1.997}Al_{0.003})_{\Sigma=2}O_5(OH)_{3.639}$.

Lattice parameters [$a = 43.505(6)$, $b = 9.251(1)$, $c = 7.263(1)$ Å, $\beta = 91.32(1)°$] were determined using a single-crystal diffractometer equipped with an area detector. The structure was refined using 9242 independent reflections, obtaining a final $R_{4\sigma}$ factor of 0.0577. A continuous, wavy octahedral sheet is linked to a tetrahedral sheet with tetrahedral apices alternatively pointing **+c** and **−c**. This sheet is located on the concave side of the octahedral-sheet wave. The octahedral sheet shows normal thickness for a serpentine of this composition, and does not have any internal offset. The tetrahedral sheet inverts its polarity through six- and eight-membered tetrahedral rings (6- and 8-reversals). Between reversals, 6-membered rings are distorted toward ditrigonal configuration, with tetrahedral rotation, α values, ranging along the wave from 4 to 13.6°. The two half-waves have curvature radii of 99.4 and 110.9 Å. Variable interlayer O-O distances occur, indicating the absence of homogeneous, continuous hydrogen bonding. The bond geometry, very similar to that of lizardite, suggests common crystal chemical and geochemical properties. The larger stability field of antigorite compared to lizardite is interpreted to arise from the occurrence of three-dimensionally connected chemical bonds.

INTRODUCTION

Antigorite is a rock-forming mineral, common in prograde regional and contact metamorphic serpentinites (e.g., Mellini et al. 1987; Wicks and O'Hanley 1988). Stable to 720 °C at 2 GPa, antigorite may carry water in subducting plates (Ulmer and Trommsdorff 1995). Antigorite is a 1:1 layer silicate, chemically and structurally related to the serpentine minerals chrysotile and lizardite. The layer is flat in lizardite (e.g., Jahanbagloo and Zoltai 1968), forms cylindrical or spiral tubes in chrysotile (Whittaker 1953, 1956), and assumes a modulated wave-like shape in antigorite (Zussman 1954). Antigorite is not a serpentine polymorph strictu sensu, because of the discrete $Mg(OH)_2$ depletion as indicated by the formula $M^{VI}_{3m-3}T^{IV}_{2m}O_{5m}(OH)_{4m-6}$ (with M = Mg, Fe, Ni, Al; T = Si, Al; m = number of unique tetrahedra along the wavelength). Structural details have been controversial (e.g., Viti 1997; Dodony et al. 2002) and, despite the geologic importance of the mineral, no detailed understanding of non-stoichiometry, crystal chemical behavior under different *P-T-X* conditions, physical properties, mineral stability, and phase relationships is available.

Reliable structural data for antigorite are difficult to obtain. Attempts to perform structure analysis using powder diffraction have been fruitless, probably because of the weak, closely spaced satellite diffractions (Uehara and Shirozu 1985). Electron diffraction and high-resolution transmission electron microscopy (HRTEM) cause beam damage and quantitative image interpretation is hampered by even small crystal tilt or microscope misalignment (Yada 1979; Otten 1993; Dodony et al. 2002; Grobéty 2003). Furthermore, crystals are frequently faulted by

(001) twinning, *b*/3 stacking disorder is common, and polytypic and polysomatic intergrowths occur. Because of all that, for a long time X-ray diffraction and HRTEM have been unable to obtain a satisfactory, quantitative three-dimensional structure model (Mellini et al. 2002). Only recently Dodony et al. (2002) and Grobéty (2003) have published HRTEM images that seem sufficient to assure satisfactory structural interpretation. However, their results are conflicting, as the former denies and the latter demonstrates the presence of eight-membered tetrahedral rings (i.e., the so-called 8-reversals).

The complex, modulated structure of antigorite was first described by Aruja (1945), who determined unit cell and symmetry for antigorite ($m = 17$) from Cropp River, Mikonui, New Zealand. Aruja interpreted the incoherent scattering (streaks) on 0*kl* rows as relating to *b*/3 stacking disorder. He also reported modulated X-ray diffraction intensities with maxima every 17 superlattice spots, and he correctly compared antigorite with chrysotile, but incorrectly concluded that antigorite has a chain structure.

Robinson and Shaw (1952) reported that Professor L. Onsager (Yale University) proposed that the data of Aruja could be interpreted as a 1:1 layer structure with inversions every 43.4 Å in the **a** direction. Thus, the bending of the layers produces an undulating plate and not a chrysotile-like cylindrical habit. Instead of the normal hexagonal array of Si, he suggested that they form rectangles and octagons in projection at the inversion line. The distance between successive inversions is 8.5 times the *a* dimension of the Si-O network (5.2 Å). However this distance has only sixteen octahedra and not seventeen as normally would be the case in a planar structure.

The Onsager model was tested by Zussman (1954). He

* E-mail: gcapitani@unisi.it

performed optical transforms in a so-called "diffraction spectroscope" and compared three differently modulated structures ($m = 17$). The trail models were the Onsager "alternating-wave" structure, Zussman's "rectified-wave", and a "zigzag" model. Reliable optical transforms were obtained only for the first two models. Zussman (1954) further supported those models, by publishing observed compositions matching the $3Mg(OH)_2$ depletion predicted by the Onsager model. By that time, the presence of 48, rather than 51, octahedral cations per 34 tetrahedral cations was well established.

The Onsager model was confirmed by Kunze (1956, 1958). He assigned the *Pm* space group to antigorite ($m = 17$), built a trial model ("the double half-wave structure") starting from chrysotile, and used X-ray amplitudes to calculate one-dimensional *h*00 and two-dimensional *h*0*l* Fourier syntheses. The monumental work of Kunze was mostly theoretical and based upon a limited experimental data set. The Kunze model resulted in poorly constrained one-dimensional and two-dimensional refinements, with discrepancy factors as high as 0.235 and 0.434, respectively. Thus only the gross features of these models deserve to be considered. Details that require assessment include the claimed presence of octahedral offsets, the large octahedral sheet thickness, and the estimated curvature radius of the wave.

In the late 1950s, electron-diffraction data revealed variable modulations. In addition to the basic 43 Å periodicity ($m = 17$), other *a* values indicating integer values of *m* were observed (Zussman et al. 1957; Brindley et al. 1958; Chapman and Zussman 1959; Kamiya et al. 1959; Kunze 1960, 1961). Based on electron-diffraction data, Buseck and Cowley (1983) described antigorite as a modulated incommensurate structure. Structural modulation in antigorite was later described by polysomatism theory, alternatively using three (Spinnler 1985) or two modules (Ferraris et al. 1986; Mellini et al. 1987).

Although structural details, especially at wave reversals, were still controversial (e.g., Uehara and Shirozu 1985; Viti 1997; Dodony et al. 2002), the Onsager-Zussman-Kunze alternating wave became the reference model used to interpret electron diffraction and HRTEM images (Yada 1979; Yada et al. 1980; Cressey and Hutchison 1983; Spinnler et al. 1983; Spinnler 1985; Mellini et al. 1987; Hansen and O'Keeffe 1988; Wu et al. 1989; Uehara and Kamata 1994; Viti and Mellini 1996; Uehara 1998; Wunder et al. 2001; Grobéty 2003). For instance, Otten (1993) summarized the main microstructural features (polysomatic faults, modulation dislocations, polysynthetic twins, and fringe offsets) and performed HRTEM simulations based upon that structure.

From previous work on antigorite, we observed a promising specimen (Mg159) for structural analysis, from the central part of the Malenco serpentinite body (Northern Italy), which was first studied by Trommsdorff and Evans (1972). HRTEM showed extremely limited polysomatic disorder ($m = 17$ polysome, with 43.5 Å periodicity) and very rare (001) twins (Mellini et al. 1987). Because of the homogeneous chemical composition and the high structural order acquired through long metamorphic annealing, Mg159 has been used as a reference material in several serpentine studies. For instance, it was used for Mössbauer spectroscopy (that showed only octahedral iron, 85% ferrous, Peretti 1988) and as starting material in the piston-cylinder experiments by

Ulmer and Trommsdorff (1995). We now report the results of the first X-ray three-dimensional refinement of antigorite, performed using the exceptionally crystalline Mg159 ($m = 17$) antigorite polysome.

CRYSTAL DATA AND STRUCTURE REFINEMENT

The following data was derived from single crystals, selected from the 150 μm granulometric fraction of antigorite fragments, separated by Peretti (1988) using gravimetric and magnetic separation techniques.

Chemical composition

Homogeneous compositions were obtained from eleven epoxy-embedded polished crystals, using a wavelength dispersive JEOL JXA-9600 electron microprobe. Elemental intensities were collected at 15 kV, with a beam current of 10 nA, and peak and background counting times from 15 to 40 seconds. Raw data were corrected according to Bence and Albee (1968); albite (Si), plagioclase (Al), olivine (Mg), bustamite (Mn), ilmenite (Fe), chromite (Cr), and metal Ni were used as standards. The average chemical composition is SiO_2 42.75, TiO_2 0.01, Al_2O_3 1.39, Cr_2O_3 0.38, FeO 2.65, MnO 0.05, NiO 0.09, MgO 38.40, and CaO 0.03 wt% ($\Sigma = 85.75$). Recalculation by imposing the cationic contents predicted by the $M_{2.824}T_2O_5(OH)_{3.647}$ stoichiometry of the $m = 17$ polysome gives the formula: $(Mg_{2.673}Fe^{2+}_{0.098}Fe^{3+}_{0.015}Al_{0.035}Cr_{0.007}Ni_{0.003}Mn_{0.002})_{\Sigma=2.823}(Si_{1.997}Al_{0.003})_{\Sigma=2}O_5(OH)_{3.639}$, which is consistent with Peretti (1988).

Single crystal X-ray diffraction data

Several crystals, examined by Weissenberg techniques, confirmed the electron diffraction data and showed a well-ordered $m = 17$ polysome with diffraction symmetry $2/m$ and lattice parameters $a = 43.5$, $b = 9.2$, $c = 7.2$ Å, $\beta = 91°$. No systematic extinction was observed, thus indicating $P2/m$, Pm, or $P2$ as the possible space groups of Mg159 antigorite.

Diffraction intensities were collected from a selected (001) cleavage flake $165 \times 45 \times 15$ μm in size using a Bruker AXS D8 single crystal diffractometer, equipped with a SMART Apex CCD detector and working at 55 kV and 30 mA, with a crystal-to-detector distance of 8.0 cm and graphite-monochromatized $MoK\alpha$ radiation. Unit-cell dimensions were calculated from least-squares refinement of the positions of all the collected reflections. The resulting values, $a = 43.505(6)$, $b = 9.251(1)$, $c = 7.263(1)$ Å, $\beta = 91.32(1)°$, which compare favorably with the data $a = 43.54$, $b = 9.247$, $c = 7.255$ Å, $\beta = 91.29°$ obtained by Peretti (1988). According to the present data and that of Peretti (1988), calculated densities are 2.614 and 2.615 g/cm³, respectively. Aruja, (1945) determined a value of 2.60 g/cm³ measured for the Mikonui antigorite. Diffraction data were integrated and corrected for Lorentz, polarization, and background effects using the SAINT+ software version 6.02 (Bruker AXS-9/19/01). Frame widths of 0.3° in ω were used to collect three sets of 600 frames at different φ values (0°, 120°, 240°). The frames were collected with 60 s counting time. Raw intensity data were corrected for absorption using the SADABS v. 2.03 program (Sheldrick 1996).

A total of 37 379 reflections (symmetry related, multiply collected) were collected to $2\theta = 61°$. After merging in the $2/m$ Laue group, a set of 9242 unique reflections were produced, with an internal discrepancy factor among symmetry related reflections, $R_{obs} = \Sigma||F_o| - |F_o||/\Sigma[F_o]$, of 0.042. This excellent agreement factor further supports the monoclinic symmetry of Mg159 antigorite. Very weak 030, 050, 070, 090, and 0 11 0 reflections suggest the possible occurrence of 2_1 pseudo-symmetry.

Structure determination and refinement

The structures were determined in the *Pm* space group with the SIR97 direct method package (Altomare et al. 1999), which showed the entire octahedral sheet and many tetrahedral cations (T) and O atoms. By subsequent Fourier syntheses, coupled with least-squares refinement cycles using SHELX-97 (Sheldrick 1997), we located the remaining T and O atoms. However, the conventional discrepancy factor $R_{obs} = \Sigma||F_o| - |F_c|| / \Sigma|F_o|$ was quite high (near 0.36), with important ΔF residual maxima shifted by $b/3$ with respect to the T cations.

Following the study of Aruja (1945), these residual maxima were related to $b/3$ stacking disorder. These faults, common in layer silicates, are related to the $b/3$ sub-periodicity of the octahedral sheet. They consist of disordered [001] stacking sequences, with adjacent tetrahedral sheets randomly shifted by one octahedral edge (i.e., $b/3$). Stacking disorder was modeled by introducing two partial structures, consisting of supplementary Si and basal O atoms, shifted by $\pm\mathbf{b}/3$ with respect to

the basic structure, with sums of related occupancies constrained to one. We did not introduce supplementary sites for the octahedral sheet, because the octahedral atoms almost overlap at $b/3$ intervals. Modeling of the stacking faults was effective with the R_{obs} factor being reduced to 0.11. According to the refined occupancy factors, the basic structure accounts for 60% of the diffracting volume, whereas 20% is shifted by $+\mathbf{b}/3$ and 20% by $-\mathbf{b}/3$. At this stage, the refined model neatly showed the main structural features expected for the Onsager-Zussman-Kunze alternating-wave structure (in particular, both 8- and 6-reversals).

The magnesium/iron ratios of the octahedral sites were allowed to vary, obtaining very minor iron occupancies, in agreement with the chemical analyses. Hydrogen atoms were introduced and their x and y coordinates were constrained to those of the bonded O atoms. Their z coordinates were allowed to vary restraining the O-H distance to 1.0 Å. Two isotropic atomic displacement parameters were refined for the hydrogen atoms, one for the "inner" hydrogen atoms within the 1:1 layer and one for the "outer" hydrogen atoms between the 1:1 layers. Anisotropic thermal displacement parameters for the Si, Mg, and O atoms were progressively introduced (sometimes resulting in non-positive thermal ellipsoids indicating physically unreasonable shapes). Residual ΔF maxima indicated further disordered Si atoms, close to the sheet reversals and compatible with polysomatic disorder. Polysomatic disorder was modeled introducing three additional disordered T sites. The total occupancy of the disorder related T sites was restrained to 1.0 and refined to a maximum of 0.36 for individual sites. During the refinement, reflections were weighted according to the reciprocal of the squared standard deviations. Divergence was avoided by introducing geometrical constraints for the M-O and T-O bond distances, which were progressively released during the final refinement cycles.

The final discrepancy R-values were 0.0577, calculated for 5246 reflections with $F_{obs} > 4\sigma(F_{obs})$, and 0.1574 for all 9242 data; approximately 1300 independent parameters were allowed to vary during the final refinement cycles. Final atomic positional and displacement parameters are reported in Tables 1 and 2, respectively. The sites are labeled in the following way: T1 to T17 are tetrahedrally coordinated cations; A1 to A17 are apical O atoms, shared between T tetrahedra and M octahedra; B1 to B17 are silicon bonded basal O atoms, with A and B suffixes indicating special and general positions, respectively (e.g., B1A and B1B); M1 to M16 are octahedrally coordinated cations, in special (A) and general (B) positions; W1 (A and B) to W15 (A and B) and V0 to V16 are the O atoms completing the octahedral sheet, linked respectively to hydrogen atoms H1 to H15 (A and B) and I0 to I16. W and V sites represent the outer and inner hydroxyl groups, respectively. Observed and calculated structure factors are provided on request[1].

RESULTS

Structural topology

The main features of the antigorite (m =17) structure are depicted in Figure 1. The structure refinement, unit-cell metrics, and diffraction symmetry support monoclinic symmetry of the m = 17 antigorite, and not the triclinic symmetry suggested by Dodony et al. (2002).

Regular and continuous octahedral sheets (M1 to M16) are pseudo-sinusoidally developed along $\mathbf{a}$, with flexure lines every eight octahedra (between M8 and M9, and between M16 and M1). Continuous tetrahedral sheets (T1 to T17) link the concave side of the octahedral sheet, inverting polarity every nine and eight tetrahedra (i.e., between T9 and T10, and between T17 and T1).

The tetrahedral-sheet configuration is best illustrated in the (001) plane (Fig. 2). Six-membered rings, like in the basic 1:1 lizardite structure, regularly repeat until reversals, which are characterized by two possible configurations. The 6-reversals oc-

cur between T17 and T1 and consist of six-membered tetrahedral rings, but with two tetrahedra pointing in one direction (+) and four in the opposite direction (–). The 8-reversals, between T9 and T10, consist of eight-membered tetrahedral rings (four pointing + and four –) and alternate along [010] with four-membered tetrahedral rings (two pointing + and two –).

In the m = 17 antigorite polysome, the two half-waves (crystallographically independent and physically different) define asymmetric pseudo-sinusoidal modulation. Both the half-waves contain eight octahedra, but the numbers of tetrahedra differ (nine vs. eight). Therefore, we distinguish between a "short" half-wave (from T10 to T17, eight tetrahedra) from a "long" half-wave (from T1 to T9, nine tetrahedra).

This structural topology is similar to the two-dimensional model for the tetrahedra as determined by Kunze (1958), but differs by the absence of octahedral offsets in the refined model. The [001] projection of the antigorite octahedral sheet (Fig. 3) appears as any non-modulated trioctahedral layer silicate. Therefore, our refinement fits the proposal by Uehara (Uehara 1998, Table 2; Dodony et al. 2002, Fig. 13b) better than the Kunze model.

The antigorite structural modulation may be described as a double transverse and longitudinal modulation; transverse, wave-like modulation arises from a lateral [001] shift of atoms along x (Fig. 1); longitudinal modulation derives from the presence of 6- and 8-reversals (Fig. 2), that locally modify the tetrahedral sheet configuration. The simultaneous presence of two different but related modulations is illustrated in the perspective view of Figure 4.

Bond geometry

Table 3 reports the refined octahedral M-O bond distances. Most M sites (Figs. 1 and 3) coordinate three O atoms located on the outer, convex surface of the 1:1 layer (the W hydroxyl groups); another O atom (V hydroxyl group) is located on the inner, concave surface and two apical (A) O atoms are shared with the tetrahedra. In antigorite, M cations are usually connected with two O atoms and four hydroxyl groups, as in lizardite. The bonding patterns, however, change at the reversals, which are associated also with hydrogen loss. At the 6-reversal, M1A and M16A remain connected to four hydroxyl groups, but M1B and M16B are connected to only three hydroxyl groups. At the 8-reversal, M9B is connected to four hydroxyl groups and M9A to two hydroxyl groups. Taking into account site multiplicities, we conclude that four and two hydrogen atoms are omitted close to the 6- and 8-reversal, respectively.

The M-O bond pattern defines slightly distorted octahedra or, more precisely, trigonal antiprisms. Over 32 independently refined M sites, the <M-O> average distance is 2.088 Å; individual bonds range from 2.005 Å (M13B-W12B) to 2.207 Å (M5B-A6). The values of individual bond distances follow regular patterns. In particular, M-W distances (i.e., outer hydroxyl groups) are shorter than M-V (i.e., with inner hydroxyl groups) and M-A distances, with average values of 2.047, 2.118, and 2.126 Å, respectively. The bonding pattern does not change significantly within the two half-waves, as indicated by the similar average values for the two half-waves (i.e., columns <M1-M8> and <M9-M16> of Table 3).

The M-O antigorite bond pattern is almost indistinguishable

TABLE 1. Atomic coordinates ($\times 10^4$) and equivalent isotropic displacement parameters ($\text{Å}^2 \times 10^3$) for Mg[159] antigorite

	x	y	z	U_{eq}		x	y	z	U_{eq}
T1	216 (1)	1663 (7)	5046 (7)	9 (1)	A17	9847 (1)	3322 (9)	−42 (11)	25 (2)
T2	817 (1)	3342 (5)	4677 (5)	9 (1)	B1A	230 (2)	0	5783 (13)	37 (2)
T3	1412 (1)	1654 (5)	4398 (4)	7 (1)	B1B	569 (3)	2453 (18)	5890 (20)	32 (5)
T4	2007 (1)	3341 (5)	4294 (4)	6 (1)	B2A	810 (2)	5000	5473 (10)	13 (2)
T5	2610 (1)	1664 (5)	4272 (4)	6 (1)	B2B	1138 (2)	2598 (16)	5281 (13)	28 (2)
T6	3214 (1)	3340 (5)	4311 (4)	5 (1)	B3A	1393 (2)	0	5201 (10)	6 (1)
T7	3819 (1)	1661 (5)	4446 (4)	5 (1)	B3B	1721 (2)	2409 (13)	5157 (12)	23 (2)
T8	4418 (1)	3336 (5)	4691 (4)	8 (1)	B4A	1993 (2)	5000	5093 (11)	12 (2)
T9	5010 (1)	1654 (6)	5050 (5)	5 (1)	B4B	2315 (2)	2624 (14)	5105 (11)	19 (2)
T10	5575 (1)	1646 (5)	−2312 (4)	7 (1)	B5A	2587 (2)	0	5068 (9)	10 (2)
T11	6169 (1)	3339 (5)	−1915(5)	6 (1)	B5B	2922 (2)	2381 (13)	5141 (10)	15 (2)
T12	6764 (1)	1663 (5)	−1725 (4)	5 (1)	B6A	3197 (2)	5000	5137 (9)	6 (1)
T13	7367 (1)	3326 (5)	−1613 (4)	6 (1)	B6B	3527 (2)	2614 (13)	5243 (10)	12 (2)
T14	7970 (1)	1655 (5)	−1591 (4)	4 (1)	B7A	3791 (2)	0	5262 (8)	6 (1)
T15	8574 (1)	3332 (5)	−1652 (5)	7 (1)	B7B	4130 (2)	2330 (12)	5383 (10)	9 (2)
T16	9173 (1)	1656 (5)	−1848 (5)	7 (1)	B8A	4369 (2)	5000	5452 (9)	12 (1)
T17	9766 (1)	3353 (6)	−2226 (6)	12 (1)	B8B	4721 (2)	2664 (13)	5673 (13)	28 (2)
M1A	301 (1)	0	1254 (9)	15 (1)	B9A	4936 (2)	0	5732 (13)	18 (2)
M1B	302 (1)	3336 (4)	1245 (7)	15 (1)	B9B	5290 (2)	2237 (10)	−3540 (16)	23 (2)
M2A	931 (1)	5000	850 (8)	17 (1)	B10A	5666 (9)	0	−3060 (40)	21 (11)
M2B	930 (1)	1657 (4)	829 (6)	15 (1)	B10B	5865 (2)	2647 (13)	−2931 (11)	19 (2)
M3A	1556 (1)	0	608 (8)	17 (1)	B11A	6190 (3)	5000	−2700 (30)	154 (10)
M3B	1554 (1)	3336 (4)	594 (5)	12 (1)	B11B	6465 (2)	2470 (13)	−2606 (12)	19 (2)
M4A	2179 (1)	5000	488 (7)	12 (1)	B12A	6767 (4)	0	−2430 (30)	145 (10)
M4B	2177 (1)	1667 (4)	494 (5)	16 (1)	B12B	7053 (2)	2533 (14)	−2457 (13)	20 (2)
M5A	2798 (1)	0	483 (6)	7 (1)	B13A	7369 (3)	5000	−2420 (20)	80 (5)
M5B	2795 (1)	3335 (4)	482 (4)	13 (1)	B13B	7654 (2)	2440 (13)	−2397 (12)	18 (2)
M6A	3420 (1)	5000	554 (6)	11 (1)	B14A	7978 (4)	0	−2460 (30)	94 (6)
M6B	3419 (1)	1667 (4)	552 (4)	8 (1)	B14B	8251 (2)	2586 (14)	−2432 (11)	15 (2)
M7A	4044 (1)	0	727 (7)	11 (1)	B15A	8598 (5)	5000	−2480 (20)	91 (6)
M7B	4042 (1)	3334 (4)	716 (5)	11 (1)	B15B	8848 (2)	2375 (14)	−2524 (12)	18 (2)
M8A	4672 (1)	5000	1009 (7)	12 (1)	B16A	9155 (4)	0	−2760 (20)	89 (6)
M8B	4670 (1)	1660 (4)	998 (5)	12 (1)	B16B	9431 (2)	2620 (14)	−2807 (12)	26 (2)
M9A	5298 (1)	0	1379 (8)	12 (1)	B17A	9716 (9)	5000	−3330 (60)	230 (30)
M9B	5299 (1)	3334 (4)	1380 (6)	13 (1)	B17B	0 (3)	2343 (19)	6760 (20)	73 (5)
M10A	5921 (1)	5000	1756 (8)	13 (1)	V0	117 (2)	5000	2784 (16)	21 (2)
M10B	5924 (1)	1661 (4)	1750 (5)	14 (1)	V1	746 (2)	0	2411 (13)	11 (2)
M11A	6542 (1)	0	2035 (7)	11 (1)	V2	1364 (2)	5000	2171 (11)	13 (2)
M11B	6541 (1)	3336 (4)	2046 (5)	12 (1)	V3	1987 (2)	0	2063 (12)	14 (2)
M12A	7165 (1)	5000	2174 (7)	16 (1)	V4	2608 (2)	5000	1996 (12)	14 (2)
M12B	7164 (1)	1661 (4)	2175 (5)	14 (1)	V5	3218 (2)	0	2080 (12)	12 (2)
M13A	7787 (1)	0	2254 (7)	16 (2)	V6	3832 (2)	5000	2199 (12)	13 (2)
M13B	7786 (1)	3332 (4)	2229 (4)	8 (1)	V7	4447 (2)	0	2452 (14)	17 (2)
M14A	8414 (1)	5000	2221 (6)	11 (1)	V8	5070 (2)	5000	2766 (14)	19 (2)
M14B	8414 (1)	1661 (4)	2196 (4)	10 (1)	V9	5518 (2)	5000	−39 (13)	13 (2)
M15A	9040 (1)	0	2100 (7)	8 (1)	V10	6143 (2)	0	298 (13)	12 (2)
M15B	9040 (1)	3338 (4)	2049 (5)	15 (1)	V11	6759 (2)	5000	529 (15)	16 (2)
M16A	9669 (1)	5000	1727 (8)	14 (1)	V12	7374 (2)	0	676 (14)	16 (2)
M16B	9671 (1)	1669 (4)	1721 (6)	15 (1)	V13	7992 (2)	5000	665 (14)	17 (2)
A1	121 (1)	1677 (8)	2808 (8)	12 (1)	V14	8602 (2)	0	595 (16)	25 (3)
A2	757 (2)	3328 (8)	2463 (9)	15 (1)	V15	9216 (2)	5000	346 (16)	24 (3)
A3	1376 (1)	1665 (8)	2218 (8)	10 (1)	V16	9846 (3)	0	22 (16)	27 (3)
A4	1991 (1)	3344 (8)	2140 (9)	14 (1)	W1A	479 (3)	5000	−299 (15)	25 (3)
A5	2606 (2)	1660 (8)	2065 (7)	12 (1)	W1B	483 (2)	1670 (10)	−349 (11)	25 (2)
A6	3223 (2)	3332 (8)	2175 (8)	12 (1)	W2A	1121 (2)	0	−599 (15)	18 (2)
A7	3835 (2)	1664 (8)	2241 (8)	15 (1)	W2B	1126 (1)	3320 (9)	−582 (9)	16 (1)
A8	4452 (2)	3329 (9)	2503 (9)	18 (1)	W3A	1752 (3)	5000	−805 (13)	16 (2)
A9	5078 (1)	1680 (9)	2847 (9)	15 (1)	W3B	1750 (1)	1671 (8)	−829 (8)	12 (1)
A10	5520 (2)	1664 (9)	−53 (10)	17 (1)	W4A	2384 (2)	0	−894 (12)	13 (2)
A11	6146 (1)	3338 (8)	285 (8)	11 (1)	W4B	2384 (2)	3332 (8)	−886 (7)	13 (1)
A12	6759 (1)	1670 (8)	546 (9)	14 (1)	W5A	3006 (2)	5000	−855 (11)	14 (2)
A13	7374 (1)	3326 (9)	696 (9)	15 (1)	W5B	3010 (2)	1661 (8)	−850 (7)	15 (1)
A14	7988 (1)	1667 (9)	677 (9)	17 (1)	W6A	3638 (2)	0	−750 (13)	11 (2)
A15	8602 (1)	3330 (9)	623 (8)	16 (1)	W6B	3639 (2)	3339 (8)	−754 (8)	13 (1)
A16	9221 (1)	1652 (9)	344 (11)	24 (2)	W7A	4270 (2)	5000	−486 (14)	15 (2)

Notes: U_{eq} is defined as 1/3 of the trace of the orthogonalized U_{ij} tensor. Estimated standard deviations in brackets. T = tetrahedral cations; M = octahedral cations; A = apical oxygen atoms; B = basal oxygen atoms; V and I = oxygen and hydrogen atoms forming inner hydroxyls; W and H = oxygen and hydrogen atoms forming outer hydroxyls; numbers from 1 to 17 indicate the crystallographic module in the wavy structure and the A or B letters specify special or general positions.

Table 1.–*extended*

	x		y		z		U_{eq}	
W7B	4271	(1)	1664	(8)	–531	(9)	15	(1)
W8A	4897	(2)	0		–239	(13)	11	(2)
W8B	4898	(1)	3321	(8)	–247	(9)	13	(1)
W9A	5695	(2)	0		2924	(15)	23	(3)
W9B	5698	(2)	3324	(9)	2937	(9)	20	(2)
W10A	6323	(2)	5000		3277	(13)	18	(2)
W10B	6329	(1)	1679	(8)	3267	(8)	13	(1)
W11A	6955	(2)	0		3440	(15)	19	(2)
W11B	6960	(1)	3330	(10)	3454	(10)	22	(2)
W12A	7587	(2)	5000		3526	(15)	20	(2)
W12B	7584	(1)	1688	(9)	3534	(9)	17	(2)
W13A	8215	(2)	0		3526	(15)	20	(2)
W13B	8213	(1)	3330	(9)	3501	(10)	21	(2)
W14A	8844	(2)	5000		3418	(15)	18	(2)
W14B	8845	(1)	1669	(9)	3413	(10)	20	(2)
W15A	9491	(2)	0		3195	(15)	18	(2)
W15B	9492	(1)	3331	(8)	3156	(10)	16	(1)
I0	117	(2)	5000		4170	(40)	200	(20)
I1	746	(2)	0		3790	(40)	200	(20)
I2	1364	(2)	5000		3560	(40)	200	(20)
I3	1987	(2)	0		3440	(40)	200	(20)
I4	2608	(2)	5000		3360	(40)	200	(20)
I5	3218	(2)	0		3440	(40)	200	(20)
I6	3832	(2)	5000		3570	(40)	200	(20)
I7	4447	(2)	0		3850	(40)	200	(20)
I8	5070	(2)	5000		4140	(40)	200	(20)
I9	5518	(2)	5000		–1430	(40)	200	(20)
I10	6143	(2)	0		–1090	(40)	200	(20)
I11	6759	(2)	5000		–860	(40)	200	(20)
I12	7374	(2)	0		–700	(40)	200	(20)
I13	7992	(2)	5000		–710	(40)	200	(20)
I14	8602	(2)	0		–790	(40)	200	(20)
I15	9216	(2)	5000		–1040	(40)	200	(20)
I16	9846	(3)	0		–1360	(40)	200	(20)
H1A	479	(3)	5000		–1680	(40)	82	(8)
H1B	483	(2)	1670	(10)	–1720	(40)	82	(8)
H2A	1121	(2)	0		–1980	(40)	82	(8)
H2B	1126	(1)	3320	(9)	–1970	(40)	82	(8)
H3A	1752	(3)	5000		–2180	(40)	82	(8)
H3B	1750	(1)	1671	(8)	–2220	(40)	82	(8)
H4A	2384	(2)	0		–2240	(40)	82	(8)
H4B	2384	(2)	3332	(8)	–2210	(40)	82	(8)
H5A	3006	(2)	5000		–2220	(40)	82	(8)
H5B	3010	(2)	1661	(8)	–2200	(40)	82	(8)
H6A	3638	(2)	0		–2120	(40)	82	(8)
H6B	3639	(2)	3339	(8)	–2130	(40)	82	(8)
H7A	4270	(2)	5000		–1870	(40)	82	(8)
H7B	4271	(1)	1664	(8)	–1930	(40)	82	(8)
H8A	4897	(2)	0		–1610	(40)	82	(8)
H8B	4898	(1)	3321	(8)	–1610	(40)	82	(8)
H9A	5695	(2)	0		4300	(40)	82	(8)
H9B	5698	(2)	3324	(9)	4330	(40)	82	(8)
H10A	6323	(2)	5000		4640	(40)	82	(8)
H10B	6329	(1)	1679	(8)	4660	(40)	82	(8)
H11A	6955	(2)	0		4800	(40)	82	(8)
H11B	6960	(1)	3330	(10)	4820	(40)	82	(8)
H12A	7587	(2)	5000		4880	(40)	82	(8)
H12B	7584	(1)	1688	(9)	4880	(40)	82	(8)
H13A	8215	(2)	0		4880	(40)	82	(8)
H13B	8213	(1)	3330	(9)	4850	(40)	82	(8)
H14A	8844	(2)	5000		4800	(40)	82	(8)
H14B	8845	(1)	1669	(9)	4830	(40)	82	(8)
H15A	9491	(2)	0		4590	(40)	82	(8)
H15B	9492	(1)	3331	(8)	4530	(40)	82	(8)

from lizardite. Also in lizardite, M atoms are asymmetrically coordinated, being systematically displaced from the octahedral centers toward the outer O atoms plane (Mellini and Viti 1994). Similar bond distances occur in both octahedra far from and near the reversals (i.e., M8-M9 and M1-M16). Therefore, no anomalous coordination pattern occurs, or anomalous bond distance, within the octahedral antigorite sheet. However, although similar, individual M-O bond lengths in antigorite are generally slightly larger than in lizardite. For instance, the typical M-W, M-V, and M-A distances in lizardite are close to 2.03, 2.09, and 2.12 Å (Table 4 of Mellini and Viti 1994), as compared to the 2.047, 2.118, and 2.126 Å values of Mg159 antigorite.

For the seventeen independent tetrahedral sites (Table 4), bond distances cluster at 1.553 (T6-A6) and 1.686 Å (T5-B4B). Exceptions are the anomalous 1.697 (T1-B17B), 1.795 (T1-B1B), and 1.730 Å (T17-B17A) values. We do not believe that these large values are real. These anomalous data probably result from tetrahedral disorder associated with polysomatic faulting. For completeness, we report (Table 4) values averaged over all the bond distances (column <T1-T17>), as well as the averages obtained excluding the anomalous T1 and T17 sites (columns <T2-T16>, <T2-T9>, and <T10-T16>). In the following discussion, we refer to these latter values.

The average T-O distance of antigorite is 1.632 Å, with the average apical T-A distance (1.617 Å) systematically shorter than the average basal T-B distance (1.637 Å). Although slightly smaller, the tetrahedral bonds in antigorite are similar to lizardite (apical T-O of 1.615 and basal T-O of 1.645 Å, respectively; Mellini and Viti 1994). However, the two half-waves of antigorite differ significantly, as the "long" half-wave <T2-T9> has T-A and T-B bond patterns more distorted than the "short" half-wave <T10-T16> (1.596 and 1.640 Å vs. 1.642 and 1.634 Å, respectively).

This latter feature may be real, or may be partially biased by the larger thermal motion affecting the O atoms of the "short" half-wave (Table 2). We note that Mellini and Zanazzi (1987) and Brigatti et al. (1997) considered the refined T-A bond distances of lizardite to be affected by strongly anisotropic thermal ellipsoids, which were elongated parallel to [001] because of stacking disorder.

Reversals

Wave-reversal in the $m = 17$ polysome defines two different local symmetries. Close to the origin, the tetrahedral sheet changes its polarity within six-membered tetrahedral rings, by a pseudo-2_1 local symmetry operator to generate the 6-reversals (Figs. 2 and 3). Otherwise, tetrahedral polarity change occurs by a pseudo-2 local symmetry operator, generating the 8-reversal, as well as the conjugate 4-reversal. The 2 and 2_1 local symmetry operators do not obey crystallographic restrictions. In the present setting, the 2_1 axis occurs at $x = 0$ and $x = 1$, whereas the 2 axis occurs at $x = 9/17$.

At the 8-reversal, the Si-O-Si bonds appear less distorted than at the 6-reversal. For instance, the T9-B9B-T10 angle is 140.9°, whereas the T1-B17B-T17 angle is 159.3°. Thus, most of the tetrahedral sheet torsion occurs at the 6-reversal (Fig. 1). This feature is important, because it is involved in the different numbers of Mg(OH)₂ depleted at the two reversals. As discussed above, four of the six hydrogen atoms are lost at the 6-reversal,

Table 2. Anisotropic displacement parameters (Å2 × 103) for Mg159 antigorite

	U_{11}	U_{22}	U_{33}	U_{23}	U_{13}	U_{12}		U_{11}	U_{22}	U_{33}	U_{23}	U_{13}	U_{12}		U_{11}	U_{22}	U_{33}	U_{23}	U_{13}	U_{12}
T1	7(2)	4(2)	17(2)	–1(2)	5(1)	0(2)	A1	17(3)	14(3)	5(2)	5(2)	1(2)	0(3)	B17A	230(40)	21(14)	450(60)	0	250(40)	0
T2	5(1)	4(1)	18(1)	–2(2)	3(1)	–2(2)	A2	29(3)	9(3)	9(2)	–1(2)	9(2)	–3(3)	B17B	54(6)	20(6)	149(15)	–18(7)	66(8)	10(5)
T3	8(1)	5(1)	8(1)	1(1)	1(1)	1(2)	A3	20(3)	1(3)	10(3)	–1(2)	7(2)	1(3)	W1A	26(6)	25(7)	25(5)	0	1(5)	0
T4	7(1)	6(1)	6(1)	1(1)	3(1)	2(2)	A4	15(3)	1(3)	25(3)	0(3)	9(3)	1(3)	W1B	17(3)	25(4)	32(4)	3(4)	8(3)	–3(4)
T5	6(1)	10(1)	2(1)	–1(1)	1(1)	1(2)	A5	32(4)	4(3)	0(2)	0(2)	0(2)	5(3)	W2A	11(5)	18(6)	25(5)	0	1(4)	0
T6	6(1)	6(1)	4(1)	0(1)	–2(1)	–1(2)	A6	25(3)	8(3)	3(2)	7(2)	5(2)	3(3)	W2B	13(3)	21(4)	15(3)	1(3)	5(2)	5(3)
T7	8(1)	2(1)	6(1)	1(1)	–2(1)	1(2)	A7	25(3)	10(3)	10(3)	4(3)	6(3)	4(3)	W3A	32(6)	9(5)	8(4)	0	8(4)	0
T8	9(1)	7(1)	8(1)	2(1)	–2(1)	1(2)	A8	18(3)	15(3)	21(3)	–1(3)	5(3)	–6(3)	W3B	23(3)	8(3)	5(2)	4(2)	9(2)	0(3)
T9	3(1)	5(2)	7(1)	1(2)	0(1)	1(2)	A9	10(3)	21(4)	15(3)	3(3)	6(2)	1(3)	W4A	24(6)	7(5)	7(4)	0	3(4)	0
T10	2(1)	8(1)	10(1)	3(1)	–1(1)	3(2)	A10	20(3)	7(3)	25(3)	0(3)	–2(3)	4(3)	W4B	31(4)	6(3)	3(2)	2(2)	1(2)	2(3)
T11	2(1)	4(1)	12(1)	–1(2)	–1(1)	2(2)	A11	8(3)	12(3)	11(3)	–5(3)	–7(2)	0(3)	W5A	31(6)	12(5)	0(4)	0	–1(4)	0
T12	2(1)	7(1)	8(1)	2(1)	3(1)	2(2)	A12	1(2)	13(3)	29(3)	–2(3)	–5(2)	4(3)	W5B	36(4)	9(3)	0(2)	6(2)	5(3)	2(3)
T13	3(1)	3(1)	11(1)	4(1)	1(1)	–1(2)	A13	0(2)	20(3)	27(3)	9(3)	–2(2)	–4(3)	W6A	15(5)	9(5)	10(4)	0	5(4)	0
T14	3(1)	2(1)	9(1)	0(1)	–1(1)	2(2)	A14	0(2)	23(4)	28(4)	1(3)	–1(2)	0(3)	W6B	27(3)	9(3)	2(2)	–1(2)	3(2)	–2(3)
T15	2(1)	5(1)	13(1)	–4(2)	–1(1)	–4(2)	A15	13(3)	23(4)	12(3)	0(3)	–7(2)	5(3)	W7A	15(5)	8(5)	21(5)	0	–2(4)	0
T16	3(1)	8(1)	9(1)	0(1)	4(1)	–1(2)	A16	1(3)	23(4)	47(4)	–3(4)	–10(3)	0(3)	W7B	19(3)	4(3)	23(3)	7(3)	7(3)	3(3)
T17	10(1)	8(2)	18(2)	–1(2)	7(1)	–3(2)	A17	5(3)	16(4)	55(4)	0(4)	–3(3)	–4(3)	W8A	10(5)	6(5)	15(5)	0	–3(4)	0
M1A	10(2)	9(2)	26(2)	0	1(2)	0	B1A	51(7)	22(5)	36(5)	0	–7(4)	0	W8B	13(3)	4(3)	21(3)	–2(3)	0(3)	4(3)
M1B	9(1)	9(1)	28(1)	2(2)	–1(1)	–1(2)	B1B	12(6)	29(9)	56(10)	–6(7)	25(6)	–11(6)	W9A	15(5)	25(7)	30(6)	0	10(5)	0
M2A	10(2)	11(3)	29(3)	0	4(2)	0	B2A	18(4)	14(4)	8(3)	0	3(3)	0	W9B	18(3)	29(4)	14(3)	0(3)	5(3)	2(4)
M2B	11(1)	8(2)	25(2)	2(1)	5(1)	0(2)	B2B	20(4)	45(6)	20(4)	10(4)	2(4)	–3(4)	W10A	23(6)	21(6)	10(5)	0	5(4)	0
M3A	12(2)	10(3)	30(3)	0	4(2)	0	B3A	2(3)	4(3)	11(3)	0	–3(2)	0	W10B	10(3)	21(4)	9(3)	6(3)	–2(2)	3(3)
M3B	8(1)	8(2)	18(2)	–1(1)	2(1)	0(1)	B3B	37(5)	13(5)	20(4)	6(3)	10(4)	–2(4)	W11A	7(5)	16(6)	34(6)	0	–1(4)	0
M4A	9(2)	8(3)	19(3)	0	2(2)	0	B4A	14(4)	8(4)	12(3)	0	–10(3)	0	W11B	8(3)	22(4)	36(4)	–2(4)	–1(3)	–2(3)
M4B	10(2)	8(2)	30(2)	–2(2)	5(1)	0(2)	B4B	23(4)	22(5)	12(4)	–6(3)	2(3)	0(4)	W12A	0(4)	22(4)	37(6)	0	0(4)	0
M5A	14(3)	5(3)	3(2)	0	0(2)	0	B5A	27(4)	4(4)	0(3)	0	4(3)	0	W12B	10(3)	22(4)	30(4)	6(3)	–1(2)	3(3)
M5B	14(2)	14(2)	12(2)	2(1)	3(1)	–2(2)	B5B	20(4)	22(4)	4(3)	4(3)	4(3)	–6(3)	W13A	10(5)	18(6)	32(6)	0	–7(5)	0
M6A	18(3)	9(3)	7(2)	0	0(2)	0	B6A	12(3)	0(3)	5(3)	0	–6(3)	0	W13B	4(3)	26(4)	35(4)	2(4)	0(3)	3(3)
M6B	15(2)	6(2)	3(1)	0(1)	1(1)	3(2)	B6B	9(3)	22(4)	3(3)	–3(3)	1(3)	–3(3)	W14A	13(5)	14(6)	27(6)	0	–4(4)	0
M7A	16(2)	7(2)	10(2)	0	5(2)	0	B7A	17(3)	0(3)	0(2)	0	1(2)	0	W14B	11(3)	19(4)	29(4)	–4(3)	–14(3)	–3(3)
M7B	14(1)	8(2)	11(1)	3(1)	4(1)	0(1)	B7B	10(3)	9(4)	8(3)	–2(2)	3(3)	–7(3)	W15A	9(5)	13(6)	30(6)	0	–9(4)	0
M8A	12(2)	10(3)	12(2)	0	5(2)	0	B8A	25(4)	8(3)	3(2)	0	–3(2)	0	W15B	14(3)	2(3)	32(4)	–1(3)	–5(3)	2(3)
M8B	17(2)	6(2)	13(1)	1(1)	7(1)	2(1)	B8B	21(4)	17(5)	45(6)	–21(4)	–13(4)	–1(4)	V0	15(5)	0(5)	48(7)	0	–1(5)	0
M9A	13(2)	9(2)	15(2)	0	2(1)	0	B9A	13(4)	15(5)	25(4)	0	5(3)	0	V1	17(5)	4(4)	10(4)	0	–2(4)	0
M9B	8(1)	13(1)	19(1)	1(2)	1(1)	2(2)	B9B	18(3)	15(3)	36(4)	–7(5)	–13(2)	4(5)	V2	37(6)	1(4)	1(4)	0	2(4)	0
M10A	5(2)	7(2)	26(3)	0	–4(2)	0	B10A	60(30)	0(14)	0(12)	0	–21(14)	0	V3	26(6)	4(5)	11(4)	0	8(4)	0
M10B	5(1)	10(2)	26(2)	–1(2)	–3(1)	2(1)	B10B	15(3)	32(5)	11(4)	–15(3)	–1(3)	8(4)	V4	31(6)	5(5)	6(4)	0	–6(4)	0
M11A	0(2)	12(3)	21(3)	0	0(2)	0	B11A	20(7)	220(30)	220(20)	0	–5(11)	0	V5	25(6)	7(5)	5(4)	0	6(4)	0
M11B	3(1)	13(2)	20(2)	–1(1)	–1(1)	–3(1)	B11B	20(4)	11(4)	25(4)	4(3)	–10(3)	–11(3)	V6	23(6)	10(5)	6(4)	0	–4(4)	0
M12A	6(2)	14(3)	28(3)	0	0(2)	0	B12A	36(9)	260(30)	139(18)	0	–7(10)	0	V7	12(5)	12(6)	27(5)	0	3(4)	0
M12B	1(1)	9(2)	31(2)	–4(1)	–1(1)	1(1)	B12B	17(4)	17(5)	25(4)	–4(3)	–2(3)	–1(3)	V8	13(5)	22(6)	23(5)	0	–2(4)	0
M13A	8(2)	12(3)	27(3)	0	–2(2)	0	B13A	50(9)	73(13)	118(14)	0	3(9)	0	V9	22(5)	7(5)	10(4)	0	6(4)	0
M13B	4(1)	7(2)	13(2)	1(1)	–3(1)	–2(1)	B13B	13(3)	16(4)	26(4)	10(3)	–5(3)	–17(3)	V10	9(5)	14(5)	12(4)	0	4(4)	0
M14A	13(2)	10(3)	11(2)	0	–3(2)	0	B14A	41(8)	97(14)	143(17)	0	10(10)	0	V11	1(4)	11(5)	35(6)	0	2(4)	0
M14B	11(2)	8(2)	10(2)	2(1)	–3(1)	1(1)	B14B	4(3)	28(5)	12(4)	6(3)	–4(3)	–10(3)	V12	0(4)	19(6)	29(6)	0	–4(4)	0
M15A	8(2)	5(2)	10(2)	0	–6(2)	0	B15A	134(15)	46(11)	93(13)	0	55(11)	0	V13	0(4)	25(6)	26(6)	0	8(4)	0
M15B	10(1)	9(2)	26(2)	–1(1)	–4(1)	1(1)	B15B	9(3)	27(5)	17(4)	–10(3)	–9(3)	13(3)	V14	2(5)	30(7)	42(7)	0	–6(5)	0
M16A	10(2)	7(2)	25(2)	0	–7(2)	0	B16A	94(13)	90(14)	80(12)	0	–25(10)	0	V15	5(5)	17(6)	49(7)	0	7(5)	0
M16B	10(1)	12(2)	24(2)	2(2)	–5(1)	0(1)	B16B	44(5)	25(5)	10(3)	16(3)	–8(3)	–28(4)	V16	21(6)	32(7)	29(6)	0	2(5)	0

Notes: The anisotropic displacement factor exponent takes the form: $-2\pi^2(h^2a^{*2}U_{11} + k^2b^{*2}U_{22} + l^2c^{*2}U_{33} + 2hka^*b^*U_{12} + 2hla^*c^*U_{13} + 2klb^*c^*U_{23})$. Estimated standard deviations in brackets.

whereas only two hydrogen atoms are lost at the 8-reversal. By imposing local charge balance, two Mg atoms would be expected to be lost at the 6-reversal and one Mg atom at the 8-reversal. Indeed, Figure 5 illustrates how at the 6-reversal the apical O atom A1 deviates by $2h/3$ with respect to the not reversed position (dashed), and at the 8-reversal the apical O atom A10 deviates by $h/3$ with respect to the not reversed position, thus destroying an octahedral slab with total width h.

Thickness of the tetrahedral and octahedral sheets

Wicks and O'Hanley (1988) summarized data on the thickness of the tetrahedral and octahedral sheets in serpentine minerals. In lizardite, the values were near to 2.21–2.22 Å and 2.10–2.12 Å for the tetrahedral and octahedral sheets, respectively. In the two-dimensional antigorite structure of Kunze (1958), a similar thickness of 2.22 Å was found for the tetrahedral sheet, whereas the octahedral sheet was believed to have an anomalous 2.44 Å value. Therefore, they suggested that the latter possessed some unique features. The present refinement shows that the antigorite tetrahedral sheet ranges in thickness from 2.162 to 2.307 Å (Table 5, thickness values at T4 and T10, respectively) thus matching lizardite. The octahedral sheet thickness (Table 6) was calculated at different locations of the layer, as distance between least-squares planes through O atoms. Values range between 2.057 Å at M12 and 2.159 Å at M9, thus matching the 2.10–2.12 lizardite range. Therefore, we conclude that no unique feature occurs in the antigorite octahedral sheet.

Curvature radii and modulation amplitude

The wave-like modulation of antigorite may be described in two different but related ways. Wicks and O'Hanley (1988) and Grobéty (2003) emphasize the curled layers, which are described

TABLE 3. Bond lengths (Å) for octahedral sites in Mg159 antigorite (selected mean values at bottom; estimated standard deviations in parentheses)

M1A-	M3A-	M5A-	M7A-	M9A-	M11A-	M13A-	M15A-
-A1 2.084 (8)	-W3B 2.059 (7)	-W4A 2.040(10)	-W6A 2.042(11)	-W9A 2.039(12)	-W10B 2.027 (7)	-W12B 2.029 (8)	-W14B 2.013 (8)
-A1 2.084 (8)	-W3B 2.059 (7)	-W5B 2.046 (7)	-W7B 2.054 (7)	-W8A 2.082(10)	-W10B 2.027 (7)	-W12B 2.029 (8)	-W14B 2.013 (8)
-V1 2.093(11)	-W2A 2.065 (11)	-W5B 2.046 (7)	-W7B 2.054 (7)	-A10 2.105 (8)	-W11A 2.045(10)	-W13A 2.060(11)	-W15A 2.099 (10)
-W1B 2.100 (9)	-A3 2.095 (7)	-A5 2.103 (7)	-A7 2.109 (7)	-A10 2.105 (8)	-A12 2.119 (8)	-V12 2.106(10)	-A16 2.152 (9)
-W1B 2.100 (9)	-A3 2.095 (7)	-A5 2.103 (7)	-A7 2.109 (7)	-A9 2.125 (8)	-A12 2.119 (8)	-A14 2.123 (8)	-A16 2.152 (9)
-V16 2.154(12)	-V3 2.133 (11)	-V5 2.140(10)	-V7 2.134(11)	-A9 2.125 (8)	-V10 2.122(10)	-A14 2.123 (8)	-V14 2.173 (10)

M1B-	M3B-	M5B-	M7B-	M9B-	M11B-	M13B-	M15B-
-W1A 2.065 (8)	-W2B 2.029 (7)	-W4B 2.026 (7)	-W6B 2.031 (7)	-W9B 2.051 (7)	-W10B 2.007 (8)	-W12B 2.005 (8)	-W14A 2.028 (8)
-V0 2.074 (8)	-W3A 2.047 (7)	-W5A 2.048 (7)	-W7A 2.040 (7)	-W8B 2.083 (7)	-W10A 2.027 (7)	-W12A 2.013 (7)	-W14B 2.030 (9)
-A1 2.075 (7)	-W3B 2.053 (7)	-W5B 2.061 (7)	-W7B 2.059 (7)	-V9 2.096 (7)	-W11B 2.068 (7)	-W13B 2.056 (7)	-W15B 2.107 (7)
-W1B 2.092 (9)	-V2 2.098 (7)	-V4 2.071 (7)	-V6 2.101 (7)	-V8 2.103 (8)	-A11 2.118 (6)	-A13 2.088 (6)	-V15 2.128 (7)
-A2 2.151 (7)	-A3 2.102 (7)	-A5 2.108 (7)	-A7 2.113 (8)	-A10 2.108 (8)	-A12 2.122 (8)	-A14 2.113 (8)	-A15 2.145 (6)
-A17 2.170 (7)	-A4 2.186 (7)	-A6 2.207 (7)	-A8 2.183 (7)	-A9 2.109 (8)	-V11 2.127 (8)	-V13 2.126 (7)	-A16 2.153 (9)

M2A-	M4A-	M6A-	M8A-	M10A-	M12A-	M14A-	M16A-
-W2B 2.064 (8)	-W4B 2.052 (7)	-W6B 2.051 (7)	-W7A 2.039(10)	-W9B 2.030 (8)	-W11B 2.022 (8)	-W13B 2.014 (8)	-W15B 2.023 (8)
-W2B 2.064 (8)	-W4B 2.052 (7)	-W6B 2.051 (7)	-W8B 2.061 (7)	-W9B 2.030 (8)	-W11B 2.022 (8)	-W13B 2.014 (8)	-W15B 2.023 (8)
-A2 2.093 (8)	-W3A 2.062 (12)	-W5A 2.053(10)	-W8B 2.061 (7)	-W10A 2.047(11)	-W12A 2.062(10)	-W14A 2.042(11)	-V0 2.079 (11)
-A2 2.093 (8)	-A4 2.122 (7)	-V6 2.130(10)	-V8 2.127(11)	-A11 2.124 (8)	-A13 2.103 (7)	-A15 2.108 (8)	-A17 2.169 (9)
-V2 2.097(11)	-A4 2.122 (7)	-A6 2.133 (7)	-A8 2.129 (8)	-A11 2.124 (8)	-A13 2.103 (7)	-A15 2.108 (8)	-A17 2.169 (9)
-W1A 2.116(12)	-V4 2.142(10)	-A6 2.133 (7)	-A8 2.129 (8)	-V9 2.160(10)	-V11 2.112(10)	-V13 2.137(10)	-V15 2.191 (11)

M2B-	M4B-	M6B-	M8B-	M10B-	M12B-	M14B-	M16B-
-W2A 2.039 (8)	-W4B 2.057 (8)	-W5B 2.028 (7)	-W7B 2.041 (7)	-W9A 2.028 (7)	-W11A 2.017 (8)	-W13A 2.021 (8)	-W15B 2.023 (8)
-W2B 2.046 (8)	-W4A 2.061 (7)	-W6A 2.057 (7)	-W8A 2.043 (7)	-W9B 2.028 (9)	-W11B 2.018 (9)	-W13B 2.021 (9)	-W15A 2.045 (8)
-V1 2.085 (7)	-W3B 2.070 (7)	-W6B 2.062 (7)	-W8B 2.049 (7)	-W10B 2.058 (6)	-W12B 2.058 (6)	-W14B 2.054 (6)	-A1 2.095 (6)
-A2 2.098 (8)	-V3 2.098 (7)	-V5 2.102 (7)	-V7 2.112 (7)	-V10 2.105 (7)	-A12 2.100 (6)	-A15 2.099 (8)	-V16 2.130 (8)
-W1B 2.106 (7)	-A4 2.131 (8)	-A6 2.128 (7)	-A8 2.128 (8)	-A11 2.128 (7)	-A13 2.100 (8)	-V14 2.104 (8)	-A17 2.147 (8)
-A3 2.169 (7)	-A5 2.165 (7)	-A7 2.165 (7)	-A9 2.200 (7)	-A10 2.166 (7)	-V12 2.105 (8)	-A14 2.133 (6)	-A16 2.175 (6)

	<M1-M16>	<M2-M15>	<M1-M8>	<M9-M16>	<AAVWWW>	<AAVVWW>	<AAAVWW>	<AAAAWW>
<M-O>	2.088 (3)	2.085 (4)	2.091 (5)	2.084 (6)	2.084 (4)	2.101(11)	2.104(15)	2.097 (14)
<M-A>	2.126 (3)	2.125 (4)	2.128 (4)	2.124 (4)	2.126 (4)	2.121(16)	2.136(15)	2.115 (6)
<M-V>	2.118 (4)	2.117 (5)	2.111 (7)	2.124 (7)	2.118 (5)	2.119(18)	2.102(28)	- -
<M-W>	2.047 (2)	2.046 (3)	2.057 (3)	2.037 (4)	2.045 (3)	2.067(15)	2.056(15)	2.061 (22)
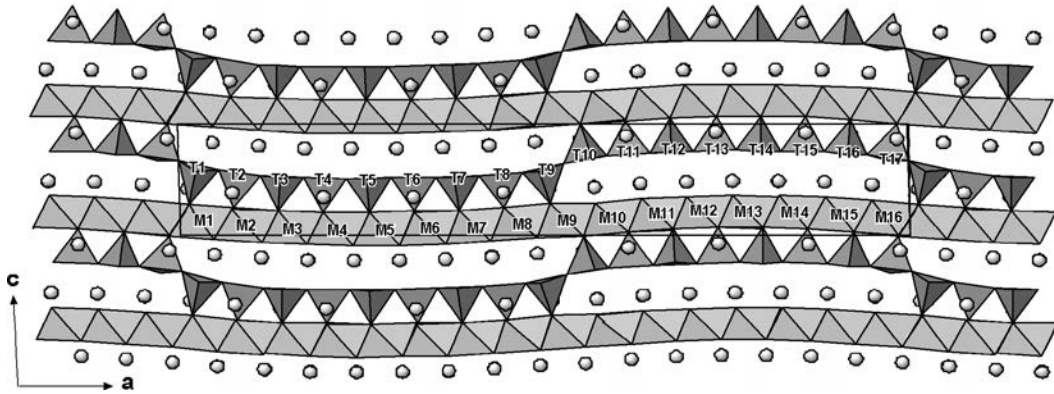
FIGURE 1. [010] projection of the modulated crystal structure of the $m = 17$ antigorite polysome. A long half-wave (T1 to T9) alternates with a short half-wave (T10 to T17). The tetrahedral wave is linked to the concave side of a continuous, corrugated octahedral sheet (M sites). Circles represent hydrogen atoms. The [001] transverse modulation is evident as wave-shaped 1:1 layer.

by curvature radius and aperture angle. Alternatively, wave-like modulation may be described by modulation wavelength, (i.e., the *a* periodicity) and modulation amplitude.

The asymmetrical shape of the alternating wave introduces an additional asymmetry effect (different curvature radii and different modulation amplitudes of the two half-waves), which is consistent with the asymmetric M-O and T-O bonding patterns described above. In fact, the two half-waves of the $m = 17$ polysome are bent to different degrees, with the "long" half-wave curved slightly more than the "short" half-wave (99.4 vs.

110.9 Å) and with a larger subtended angle (13.3 vs. 10.6°). Note that T5 is laterally displaced by 0.56 Å with respect to T1 or T9, whereas T14 is displaced by 0.52 Å and by 0.46 Å with respect to T10 and T17, respectively. These refined values differ from the 36 Å radius, the 2.18 Å amplitude, and the 28.4° angle estimated by HRTEM (Dodony et al. 2002). In addition, these values neither support the assumption of a constant 20.3° aperture angle made by Kunze (1961), nor the interpretation of TEM images by Grobéty (2003).

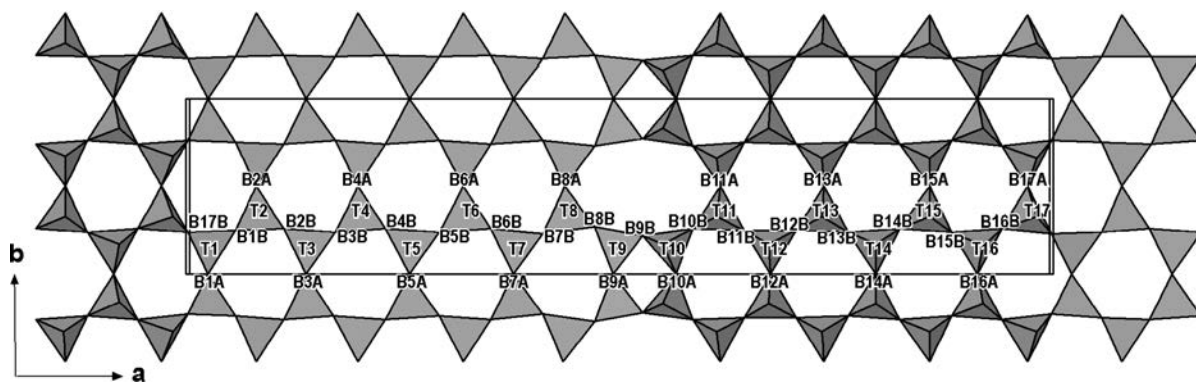The tetrahedral sheet of antigorite is on the concave side of

FIGURE 2. The modulated tetrahedral sheet of the *m* = 17 antigorite polysome as seen on (001). The sheet reverses polarity at 6- and at 8-reversals. Pseudo-symmetry operators are pseudo-2$_1$ screw axis at *x* = 0 and pseudo-2 diad axis at *x* = 1/2. Alternating 6- and 8-reversals introduce [100] longitudinal modulation.
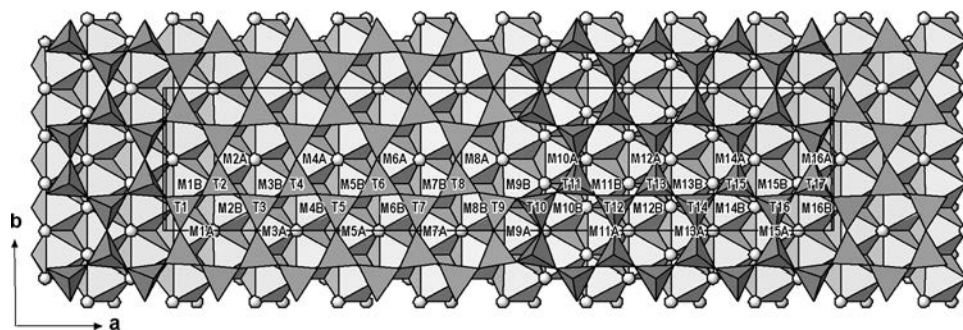

FIGURE 3. Projection on the (001) plane of the modulated 1:1 layer of the *m* = 17 antigorite polysome. Note the 6- and the 8-reversals.
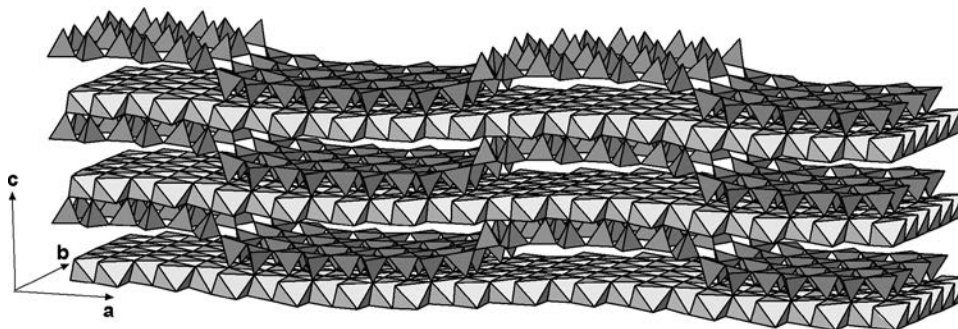

FIGURE 4. Clinographic view of the double transverse and longitudinal modulations of antigorite.

the 1:1 layer. We may consider the origin of this polarity with respect to the tetrahedral sheet on the convex side of the layer. We believe that the observed polarity of the tetrahedral sheet may be associated with repulsions between both the adjacent apical (A) O atoms and the adjacent tetrahedral cations. These repulsions are lowered by a concerted movement of the apical O atoms that force the 1:1 layer to assume a curved shape. In the case of polarity reversal, we get the wave-like antigorite structure. Otherwise, if polarity is restricted to one side of the layer, the rolled chrysotile structure is formed, necessarily having the tetrahedral sheet inside and the octahedral sheet outside.

The curvature radii as derived (99.4 and 110.9 Å) are similar to the curvature radii of chrysotile. For instance, Wicks and Whit-

taker (1975) report that the calculated ideal radius for chrysotile is 88 Å. TEM observations indicate that the maximum outer radius is close to 135–140 Å. The similarity in curvature between antigorite and chrysotile suggests that antigorite may behave as a template capable of promoting chrysotile crystallization. Assuming that the bulk antigorite structure is preserved at the surface, the (001) antigorite surface is not flat, but characterized by parallel, alternating grooves and ridges, curved according to an approximate curvature radius of 100 Å. Each half-wave may become a nucleation site to produce oriented overgrowths of chrysotile upon the (001) antigorite face, similar to those observed by Cressey et al. (1993) in "cubic" serpentine and by Baronnet et al. (2002).

TABLE 4. Bond lengths (Å) for tetrahedral sites in Mg159 (selected mean values at bottom; estimated standard deviations in parentheses)

T1-		T4-		T7-		T10-		T13-		T16-	
-B1A	1.630 (7)	-A4	1.564 (7)	-A7	1.605 (7)	-B9B	1.604 (10)	-B13B	1.605 (9)	-A16	1.601 (8)
-A1	1.668 (7)	-B4B	1.595 (9)	-B7B	1.624 (8)	-B10B	1.637 (9)	-B13A	1.656 (8)	-B16B	1.605 (10)
-B17B	1.697 (13)	-B4A	1.642 (5)	-B7A	1.653 (5)	-A10	1.663 (8)	-B12B	1.658 (10)	-B15B	1.630 (8)
-B1B	1.795 (16)	-B3B	1.648 (10)	-B6B	1.661 (9)	-B10A	1.667 (14)	-A13	1.677 (7)	-B16A	1.671 (8)

T2-		T5-		T8-		T11-		T14-		T17-	
-B2B	1.608 (10)	-A5	1.602 (6)	-A8	1.599 (7)	-A11	1.603 (7)	-B14B	1.623 (9)	-B17B	1.576 (14)
-A2	1.623 (7)	-B5B	1.626 (9)	-B8B	1.610 (9)	-B11B	1.609 (9)	-A14	1.647 (7)	-A17	1.616 (8)
-B1B	1.633 (14)	-B5A	1.649 (5)	-B7B	1.648 (9)	-B10B	1.631 (9)	-B13B	1.653 (9)	-B16B	1.653 (10)
-B2A	1.640 (5)	-B4B	1.686 (10)	-B8A	1.650 (5)	-B11A	1.641 (9)	-B14A	1.657 (8)	-B17A	1.730 (2)

T3-		T6-		T9-		T12-		T15-	
-A3	1.587 (6)	-A6	1.553 (6)	-A9	1.633 (7)	-B12B	1.593 (10)	-B15B	1.626 (9)
-B3B	1.601 (10)	-B6B	1.647 (8)	-B8B	1.640 (11)	-B11B	1.619 (9)	-B15A	1.659 (8)
-B2B	1.621 (12)	-B6A	1.651 (5)	-B9A	1.642 (6)	-B12A	1.620 (8)	B14B	1.655 (8)
-B3A	1.640 (5)	-B5B	1.674 (10)	-B9B	1.664 (11)	-A12	1.651 (7)	-A15	1.654 (7)

	<T1-T17>		<T2-T16>		<T2-T9>		<T10-T16>	
<T-O>	1.637 (5)		1.632 (4)		1.629 (6)		1.636 (5)	
<T-A>	1.620 (9)		1.617 (10)		1.596 (10)		1.642 (12)	
<T-B>	1.642 (5)		1.637 (4)		1.640 (5)		1.634 (6)	

TABLE 5. Thickness (Å) of the tetrahedral sheet at each tetrahedral module along the wave for Mg159 antigorite (standard deviations in parentheses)

T1		T6		T11		T16	
2.456	(10)	2.179	(7)	2.206	(11)	2.223	(10)
T2		T7		T12		T17	
2.257	(9)	2.222	(8)	2.209	(11)	2.278	(17)
T3		T8		T13			
2.177	(8)	2.191	(8)	2.266	(10)		
T4		T9		T14			
2.162	(8)	2.300	(9)	2.256	(10)		
T5		T10		T15			
2.207	(7)	2.307	(13)	2.253	(10)		

FIGURE 5. Drawing showing the Mg(OH)$_2$ depletion at reversal points. For explanation see text.
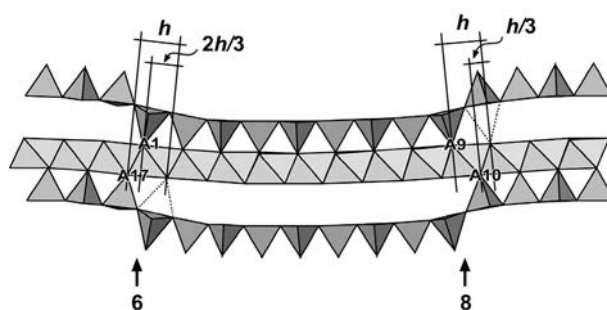
Variable layer ditrigonalization

The six-membered rings of the tetrahedral sheet of the serpentine minerals are usually distorted to a ditrigonal configuration, owing to opposite rotations of the bridging O atoms. The bridging O atoms may move away from, or toward, the nearest octahedral cations of the same layer, thus defining negative α rotation (B layer, as in lizardite-1T; Mellini 1982), or positive α rotation (A layer, as in lizardite-2H_1 and in lizardite-2H_2; Mellini and Zanazzi 1987, Brigatti et al. 1997). For lizardite, the rotation direction is controlled by interlayer hydrogen bonding.

Ditrigonalized, negatively rotated six-membered rings occur also in antigorite (Fig. 3). The rotation amount varies from ring to ring (Table 7), ranging from a minimum value of 4.0° to a maximum value of 13.6° (with α defined as the average deviation from 120°). Whereas in the "long" half-wave the magnitude of α regularly increases along x going from the 6- to the 8-reversal, irregular α distribution occurs in the "short" half-wave.

Interlayer O-O distances

In lizardite, O atoms from adjacent layers are at a distance compatible with the formation of weak hydrogen bonds: 3.03 Å in lizardite-1T from Val Sissone (Mellini 1982), 3.04 Å in lizardite-1T and 3.09 Å in lizardite-2H_1 from Coli (Mellini and Zanazzi 1987), and 3.046-3.048 Å in lizardite-1T from Elba (Mellini and Viti 1994). Although weak, they assure an efficient hydrogen-bonding network owing to the high number of adjacent bonds (one hydrogen bond per 8.2 Å^2).

In antigorite, the distance between possibly hydrogen-bonded O atoms changes along the modulation (Table 8). For the O atoms located at special positions $y = 0$ and $y = 1/2$, the interlayer O-O distance decreases from the 6- to the 8-reversal: from 3.363 Å (B1A-V1) to 2.935 Å (B9A-W8A) in the "long" half-wave, and from 3.310 Å (B16A-W15A) to 2.920 Å (B10A-W9A) in the "short" half-wave. Conversely, in the case of O atoms at general positions close to $y = 0.25$, the interlayer O-O distance shows the opposite trend: from 2.860 Å (B1B-W1B) to 3.135 Å (B9B-W8B) in the "long" half-wave, and from 3.022 Å (B16B-W15B) to 3.135 Å (B10B-W9B) in the "short" half-wave. These variable O-O distances, although in some cases assuring the conditions required for the formation of localized hydrogen bonds, prevent the formation of a homogeneous, continuous interlayer hydrogen-bonding network, in keeping with Wicks and Whittaker (1975).

Thermal motion

The refinement section reported that, in a few cases, the thermal ellipsoids are non-positive definite and thus, have no physical meaning. In particular, diagonal terms are always positive, but off-diagonal terms may not conform to required constraints (Table 2). For antigorite, the ellipsoid determination may be affected by crystal defects such as $b/3$ stacking disorder and polysomatic faults, which may affect the refinement results in two stages. During data collection, incoherent scattering smears the intensity maxima and leads to biased peak integration. During refinement, disorder

TABLE 6. Thickness (Å) of the octahedral sheet at each octahedral module and distances of the octahedral cations from the least squares planes through the outer hydroxyl oxygen atoms (starred values) and the opposite least squares planes through the inner hydroxyl and apical oxygen atoms (standard deviations in parentheses)

*1.082 (8)	M1A	1.039 (7)	*0.987 (7)	M3A	1.137 (7)	*0.978 (6)	M5A	1.155 (6)	*0.970 (6)	M7A	1.152 (7)
*1.070 (6)	M1B	1.047 (6)	*0.966 (5)	M3B	1.144 (5)	*0.978 (5)	M5B	1.149 (5)	*0.950 (5)	M7B	1.155 (5)
	2.119(3)			2.117(0)			2.130(3)			2.114(1)	
*0.976 (8)	M2A	1.106 (7)	*0.979 (7)	M4A	1.168 (7)	*0.975 (6)	M6A	1.183 (6)	*0.976 (7)	M8A	1.155 (7)
*0.973 (6)	M2B	1.113 (5)	*0.989 (5)	M4B	1.151 (5)	*0.972 (5)	M6B	1.163 (5)	*0.972 (5)	M8B	1.159 (6)
	2.084(0)			2.143(1)			2.146(1)			2.131(3)	
*1.088 (7)	M9A	*1.086 (8)	1.145 (7)	M11A	*0.938 (7)	1.145 (7)	M13A	*0.926 (8)	1.216 (7)	M15A	*0.901 (7)
*1.085 (6)	M9B	*1.064 (6)	1.159 (6)	M11B	*0.935 (5)	1.127 (6)	M13B	*0.938 (6)	1.175 (6)	M15B	*0.933 (6)
	2.162(4)			2.088(5)			2.068(0)			2.112(2)	
1.151 (7)	M10A	*0.943 (7)	1.114 (7)	M12A	*0.947 (8)	1.151 (6)	M14A	*0.909 (8)	1.195 (8)	M16A	*0.955 (8)
1.143 (5)	M10B	*0.943 (6)	1.119 (6)	M12B	*0.943 (6)	1.139 (6)	M14B	*0.935 (6)	1.173 (6)	M16B	*0.975 (6)
	2.090(0)			2.061(4)			2.067(2)			2.149(0)	

TABLE 7. Angles (°) among basal tetrahedral O atoms (estimated standard deviations in brackets) and α-values (right column) of the related ditrigonal distortion for each 6-membered ring (1 to 8 and 11 to 17) for Mg159 antigorite (α defined as the average deviation from 120°)

1)	B17B-B17A-B17B	126.6	(16)	B1B-B2A-B1B	129.9	(6)	B17B-B1B-B2A	117.3	(8)	B1B-B17B-B17A	113.1	(10)	6.0
2)	B1B-B1A-B1B	114.0	(6)	B2B-B3A-B2B	130.5	(5)	B1B-B2B-B3A	111.5	(6)	B2B-B1B-B1A	125.1	(7)	7.3
3)	B2B-B2A-B2B	114.2	(5)	B3B-B4A-B3B	127.4	(5)	B2B-B3B-B4A	112.4	(5)	B3B-B2B-B2A	126.7	(6)	7.0
4)	B3B-B3A-B3B	114.6	(5)	B4B-B5A-B4B	128.0	(5)	B3B-B4B-B5A	111.6	(5)	B4B-B3B-B3A	127.1	(5)	7.4
5)	B4B-B4A-B4B	115.0	(5)	B5B-B6A-B5B	127.5	(5)	B4B-B5B-B6A	111.4	(5)	B5B-B4B-B4A	127.4	(5)	7.4
6)	B5B-B5A-B5B	113.0	(5)	B6B-B7A-B6B	129.2	(4)	B5B-B6B-B7A	110.7	(5)	B6B-B5B-B5A	128.2	(5)	8.5
7)	B6B-B6A-B6B	113.9	(5)	B7B-B8A-B7B	134.2	(4)	B6B-B7B-B8A	107.2	(4)	B7B-B6B-B6A	128.7	(5)	10.6
8)	B7B-B7A-B7B	111.2	(4)	B8B-B9A-B8B	138.4	(5)	B7B-B8B-B9A	104.0	(5)	B8B-B7B-B7A	131.3	(5)	13.6
9)	B8B-B8A-B8B	109.3	(5)	B9B-B10A-B9B	102.4	(13)	B8B-B9B-B10A	162.4	(4)	B9B-B8B-B8A	133.9	(5)	13.9
10)	B9B-B9A-B9B	104.0	(5)	B10B-B11A-B10B	113.7	(7)	B9B-B10B-B11A	131.6	(6)	B9A-B9B-B10A	76.6	(6)	13.3
11)	B10B-B10A-B10B	141.0	(16)	B11B-B12A-B11B	120.1	(7)	B10B-B11B-B12A	123.5	(6)	B11B-B10B-B10A	105.9	(9)	9.4
12)	B11B-B11A-B11B	125.8	(7)	B12B-B13A-B12B	117.8	(7)	B11B-B12B-B13A	122.4	(6)	B12B-B11B-B11A	115.8	(6)	3.5
13)	B12B-B12A-B12B	124.1	(7)	B13B-B14A-B13B	115.9	(7)	B12B-B13B-B14A	123.9	(5)	B13B-B12B-B12A	116.0	(6)	4.0
14)	B13B-B13A-B13B	124.9	(7)	B14B-B15A-B14B	111.8	(8)	B13B-B14B-B15A	127.0	(6)	B14B-B13B-B13A	114.6	(5)	6.3
15)	B14B-B14A-B14B	127.2	(7)	B15B-B16A-B15B	116.8	(8)	B14B-B15B-B16A	125.7	(6)	B15B-B14B-B14A	112.1	(6)	6.3
16)	B15B-B15A-B15B	131.6	(8)	B16B-B17A-B16B	118.7	(13)	B15B-B16B-B17A	124.9	(9)	B16B-B15B-B15A	109.1	(6)	7.4
17)	B16B-B16A-B16B	127.2	(8)	B17B-B1A-B17B	120.5	(7)	B16B-B17B-B1A	121.7	(7)	B17B-B16B-B16A	110.4	(7)	5.1

Notes: Analogous distortion parameters, defined as the average deviation from 90° and 135°, are given for the 8-membered ring (9) and the 4-membered ring (10), respectively.

modeling may result in several approximations. For instance, $b/3$ gliding for some atoms causes near complete but not exact overlap on (001). This non-coincidence, below the resolution limit of the experiment, cannot be realistically modeled. Full account of polysomatic disorder requires considerations of not only silicon, but also basal tetrahedral O atoms. However, the basal O atoms were not modeled because of poor scattering, which resulted in an instable refinement. Finally, even rare (001) twin domains (that are very common in antigorite, Mellini et al. 1987; Otten 1993; Grobéty 2003) may affect our data to some degree.

Anisotropic displacement parameters do not appear to show problems with magnesium and silicon, nor with most of the O atoms. Anomalous anisotropic displacement parameters mostly occur for O atoms belonging to the "short" half-wave and occurring in special positions.

Polysomatism

Using the polysomatic description given for antigorite by Ferraris et al. (1986), the structure of the $m =17$ antigorite may be described as $S^+_8\,T\,S^-_7$, where S and T are the serpentine and the talc modules, respectively, and S^+ and S^- refer to polarities of the tetrahedral sheet in the two adjacent half-waves. Although polysomatism has been already used to rationalize the antigorite variability in a qualitative way (Spinnler 1985; Ferraris et al. 1986; Mellini et al. 1987), the new structural information obtained by the refinement results may allow a future quantitative application of the polysomatic relationships and the structural modulation in antigorite.

TABLE 8. Inter-layer O-O distances (Å) for Mg159 antigorite (estimated standard deviations in brackets)

B1A-V1	3.363 (14)	B1B-W1B	2.860 (17)
B2A-W1A	3.421 (13)	B2B-W2B	3.080 (12)
B3A-W2A	3.296 (13)	B3B-W3B	2.994 (11)
B4A-W3A	3.180 (11)	B4B-W4B	2.993 (10)
B5A-W4A	3.081 (11)	B5B-W5B	3.003 (10)
B6A-W5A	3.046 (11)	B6B-W6B	3.013 (10)
B7A-W6A	2.985 (11)	B7B-W7B	3.078 (10)
B8A-W7A	2.991 (12)	B8B-W8B	3.104 (12)
B9A-W8A	2.935 (13)	B9B-W8B	3.135 (14)
B10A-W9A	2.920 (3)	B10B-W9B	3.135 (10)
B11A-W10A	2.990 (3)	B11B-W10B	3.129 (10)
B12A-W11A	3.130 (2)	B12B-W11B	3.077 (12)
B13A-W12A	3.110 (2)	B13B-W12B	3.044 (11)
B14A-W13A	3.110 (2)	B14B-W13B	3.033 (11)
B15A-W14A	3.190 (2)	B15B-W14B	3.022 (11)
B16A-W15A	3.310 (2)	B16B-W15B	3.022 (11)
B17A-V0	3.350 (4)	B17B-W1B	3.000 (18)

Concluding remarks

Modular crystal chemistry. Antigorite is a complex mineral, comprised of simple octahedral and tetrahedral modules. Complexity arises from structural modulations that do not alter individual polyhedra. The wave-like antigorite superstructure

has been described as the combination of two different modulations, transverse and longitudinal waves upon a lizardite-like layer. The transverse modulation laterally displaces the atoms along the [001] direction by a limited amplitude of 0.5 Å. The longitudinal modulation arises from the occurrence of 8- and 6- reversals approximately every $a/2$ distance.

Bonding patterns. Antigorite consists of simple coordination polyhedra, repeated along the [100] direction with only minor variations with respect to the basic lizardite structure. Our results agree with previous data based upon Fourier Transform Infrared (FTIR) spectroscopy. Mellini et al. (2002) calculated that basal Si-O bonds should be shorter by 0.009 Å in antigorite with respect to lizardite, with bridging Si-O bonds "in the order of 1.638 Å rather than 1.647 Å". The value of 1.638 Å closely matches the 1.637 Å value now obtained by X-ray diffraction. In conclusion, the structural refinement of the $m = 17$ polysome shows regular silicon coordination tetrahedra and magnesium coordination octahedra. No unusual coordination occurs, such as the three-sided prisms or tetragonal bipyramids suggested by Dodony et al. (2002), and no strange effects such as octahedral offsets or anomalously thick octahedral sheets were found.

Even and odd polysomes. Disregarding unreliable details (e.g., thickness of the octahedral layer, magnesium coordination, occurrence of octahedral offset, curvature radii, etc.), the previous models appear basically correct, with regard to structural topology. In particular, we have verified the presence of 6-reversals and 8-reversals, proposed by Onsager (as quoted in Robinson and Shaw 1952), Zussman (1954) and Kunze (1958), and recently confirmed by Uehara (1998) and Grobéty (2003). This result is fortunate, in that the refinement results do no require any major modification to the many papers using the earlier models. Thus, revision to many reported chemical data or interpretations of TEM microstructures are not needed.

Conversely, our results apparently conflict with those obtained by Dodony et al. (2002), who did not find any evidence for four- and eight-membered rings, in HRTEM study of an antigorite $m = 14$ polysome ($a = 35$ Å). This apparent conflict in structure may depend upon the different parities of the two polysomes. In particular, all "odd" polysomes (e.g., $m =…13, 15, 19, 21…$) would possess the same structural features as discussed for the $m = 17$ antigorite. The omission of one tetrahedral/octahedral module would produce an "even" polysome (e.g., $m = …12, 14, 16, 18, 20…$), with the occurrence of only 6-reversals and the introduction of offsets in the octahedral sheet. We are considering such models, which will be reported elsewhere.

Reversals and Mg(OH)$_2$ loss. Because the structure of the Mg159 sample differs from the Kunze model (and the translation by Grobéty, 2003) for the structural configuration of the octahedral sheet at reversal points, the Mg(OH)$_2$ depletion does not occur at the 8-reversal only, but at the 8-reversal (two hydrogens lost, and equivalent to one Mg(OH)$_2$ unit) and at the 6-reversal (four hydrogens lost, and equivalent to two Mg(OH)$_2$ units).

Serpentine geochemistry. We conclude that the main geochemical properties, such as isomorphic substitutions, should be similar in lizardite and antigorite. Conversely, differences occur possibly related to the different hydrogen-bond network. Possible differences may involve heterovalent substitutions (e.g., Fe^{3+}, antigorite contains greater bivalent iron) or substitution of chlorine for hydroxyls (Scambelluri et al. 1997; Anselmi et al. 2000).

Antigorite stability. Different interlayer interactions, even if they do not affect the chemical properties of the individual layer, may significantly change the physical behavior of the bulk crystal. For instance, perhaps antigorite may derive a greater thermal and baric stability from a more effective interlayer interaction, such as the inversion of the tetrahedral sheet. Such inversions create a three-dimensional network of chemical bonds, which extend through the entire crystal rather than being two-dimensionally connected only, as in lizardite. Perhaps this "chemical cement" stabilizes antigorite and, with respect to lizardite, moves its phase boundaries toward higher temperature and higher pressure.

REFERENCES CITED

Altomare, A., Burla, M.C., Camalli, M., Cascarano, G., Giacovazzo, C., Guagliardi, A., Moliterni, A.G.G., Polidori, G., and Spagna, R. (1999) Sir97: a new tool for crystal structure determination and refinement. Journal of Applied Crystallography, 32, 115–119.

Anselmi, B., Mellini, M., and Viti, C. (2000) Chlorine in the Elba, Monti Livornesi and Murlo serpentines: evidence for sea-water interaction. European Journal of Mineralogy, 12, 137–146.

Aruja, E. (1945) An X-ray study of the crystal structure of antigorite. Mineralogical Magazine, 27, 65–74.

Baronnet, A., Astier, J.P., and Krasnova, N. (2003) Mècanismes de croissance des faces (001) de l' antigorite approchés par AFM et METHR. Abstracts of "Colloque annuel du GFCC. Université de Toulon et du Var. 13-15 mars 2002".

Bence, A.E. and Albee, A.L. (1968) Empirical correction factors for the electron microanalysis of silicates and oxides. Journal of Geology, 76, 382–403.

Brigatti, M.F., Galli, E., Medici, L., and Poppi, L. (1997) Crystal structure refinement of aluminian lizardite-2H_2. American Mineralogist, 82, 931–935.

Brindley, G.W., Comer, J.J., Uyeda, R., and Zussman, J. (1958) Electron optical observations with crystals of antigorite. Acta Crystallographica, 11, 99–102.

Buseck, P.R. and Cowley, J.M. (1983) Modulated and intergrowth structures in minerals and electron microscopy methods for their study. American Mineralogist, 68, 18–40.

Chapman, J.A. and Zussman, J. (1959) Further electron optical observations on crystals of antigorite. Acta Crystallographica, 12, 550–552.

Cressey, B.A. and Hutchison, J.L. (1983) Microstructure of antigorite revealed by high resolution electron microscopy. Institute of Physics Conference Series No. 68, chapter 10, 409–412.

Cressey, G., Spratt, J., and Cressey, B.A. (1993) Electron and X-ray petrography of an unusual serpentine from the Tilly Foster Mine, Brewster, New York. Canadian Mineralogist, 31, 447–458.

Dodony, I., Posfài, M., and Buseck, P.R. (2002) Revised structure models for antigorite: An HRTEM study. American Mineralogist, 87, 1443–1457.

Ferraris, G., Mellini, M., and Merlino, S. (1986) Polysomatism and the classification of minerals. Rendiconti della Società Italiana di Mineralogia e Petrografia, 41, 181–192.

Grobéty, B. (2003) Polytypes and higher-order structures of antigorite: A TEM study. American Mineralogist, 88, 27–36.

Hansen, S. and O'Keeffe, M. (1988) Oriented intergrowth of an antigorite and an arsenate mineral from Långban, Sweden. A natural composite material. Acta Crystallographica, B44, 236–242.

Jahanbagloo, C. and Zoltai, T. (1968) The crystal structure of a hexagonal Al-serpentine. American Mineralogist, 53, 14–24.

Kamiya, Y., Nonoyama, M., and Uyeda, R. (1959) Electron microscopic observation of the superlattice in serpentine. Journal of the Physical Society of Japan, 14, 1334–1346.

Kunze, V.G. (1956) Die gewellte Struktur des Antigorits, I. Zeitschrift für Kristallographie, 108, 82–107.

———(1958) Die gewellte Struktur des Antigorits, II. Zeitschrift für Kristallographie, 110, 282–320.

———(1960) Electron diffraction and moiré-patterns of the waved superlattice of antigorite. Acta Crystallographica, 13, 1093–1094.

———(1961) Antigorit. Fortschritte der Mineralogie, 39, 206–324.

Mellini, M. (1982) The crystal structure of lizardite 1T: hydrogen bonds and

polytypism. American Mineralogist, 67, 587–598.

Mellini, M. and Viti, C. (1994) Crystal structure of lizardite-1T from Elba, Italy. American Mineralogist, 79, 1194–1198.

Mellini, M. and Zanazzi, P.F. (1987) Crystal structure of lizardite -1T and lizardite –2*H*1 from Coli, Italy. American Mineralogist, 72, 943–948.

Mellini, M., Trommsdorff, V., and Compagnoni, R. (1987) Antigorite polysomatism: behaviour during progressive metamorphism. Contribution to Mineralogy and Petrology, 97, 147–155.

Mellini, M., Fuchs, Y., Viti, C., Lemaire, C., and Linares, J. (2002) Insights on the antigorite structure from Mössbauer and FTIR spectroscopies. European Journal of Mineralogy, 14, 97–104.

Otten, M.T. (1993) High-resolution electron microscopy of polysomatism and stacking defects in antigorite. American Mineralogist, 78, 75–84.

Peretti, A. (1988) Occurrence and stability of opaque minerals in the Malenco serpentinite. Ph.D. Dissertation, ETH, Zurich.

Robinson, K. and Shaw, E.R.S. (1952) Summarized proceedings of a conference on structures of silicate minerals—London November 1951. British Journal of Applied Physics, 3, 277–282.

Scambelluri, M., Piccardo, G.B., Philippot, P., Robbiano, A., and Negretti, L. (19997) High salinity fluid inclusions formed from recycled seawater in deeply subducted alpine serpentinite. Earth and Planetary Science Letters, 148, 485–499.

Sheldrick, G.M. (1997) SHELXL-97, A program for crystal structure refinement. University of Göttigen, Germany, release 97–2.

——— (1996) SADABS, Siemens area detector absorption correction software. University of Göttingen, Germany.

Spinnler, G.E. (1985) HRTEM study of antigorite, pyroxene-serpentine reactions and chlorite. Ph.D. thesis, Arizona State University, Tempe, Arizona, 248 p.

Spinnler, G.E., Veblen, D.R., and Buseck, P.R. (1983) Microstructure and defects of antigorite. Proceedings of the 41st Annual meeting of the Electron Microscopy Society of America, 41, 190–191.

Trommsdorff, V. and Evans, B.W. (1972) Progressive metamorphism of antigorite schist in the Bergell tonalite aureole (Italy). American Journal of Science, 272, 423–437.

Uehara, S. (1998) TEM and XRD study of antigorite superstructures. Canadian Mineralogist, 36, 1595–1605.

Uehara, S. and Kamata, K. (1994) Antigorite with a large supercell from Saganoseki, Oita Prefecture, Japan. Canadian Mineralogist, 32, 93–103.

Uehara, S. and Shirozu, H. (1985) Variations in chemical composition and structural properties of antigorites. Mineralogical Journal, 12, 299–318.

Ulmer, P. and Trommsdorff, V. (1995) Serpentine stability to mantle depths and subduction-related magmatism. Science, 268, 838–861.

Viti, C. (1997) Electron diffraction patterns of natural antigorites: a still unknown modulated crystal structure. In: Electron crystallography, D.L., Dorset, S., Hovmöller, X., Zou, eds., Kluwer Academic Publishers, The Netherlands, 419–422.

Viti, C. and Mellini, M. (1996) Vein antigorite from Elba Island, Italy. European Journal of Mineralogy, 8, 423–434.

Whittaker, E.J.W. (1953) The structure of chrysotile. Acta Crystallographica, 6, 747–748.

——— (1956) The structure of chrysotile. II. Clino-chrysotile. Acta Crystallographica, 9, 855–862.

Wicks, F.J. and O'Hanley, F.C. (1988) Serpentine minerals: Structures and petrology. In Mineralogical Society of America Reviews in Mineralogy, 19, 91–159.

Wicks, F.J. and Whittaker, E.J.W. (1975) A reappraisal of the structures of the serpentine minerals. Canadian Mineralogist, 13, 227–243.

Wu, X.J., Li, F.H., and Hashimoto, H.(1989) High-resolution transmission electron microscopy study of the superstructure of Xiuyan Jade and Matterhorn serpentine. Acta Crystallographica, B45, 129–136.

Wunder, B., Wirth, R., and Gottschalk, M. (2001) Antigorite: Pressure and temperature dependence of polysomatism and water content. European Journal of Mineralogy, 13, 485–495.

Yada, K. (1979) Microstructures of chrysotile and antigorite by high resolution electron microscopy. Canadian Mineralogist, 13, 227–243.

Yada, K., Tanji, T., and Nissen, H.U. (1980) Direct observation of antigorite at atomic resolution, Fourth International Conference on Asbestos, II.C/4, 347–357.

Zussman, J. (1954) Investigation of the crystal structure of antigorite. Mineralogical Magazine, 30, 498–512.

Zussman, J., Brindley, G.W., and Comer, J.J. (1957) Electron diffraction studies of serpentine minerals. American Mineralogist, 42, 133–153.